Contents lists available at ScienceDirect

Engineering Applications of Artificial Intelligence

CrossMark

Real-time embedded frame work for sEMG skeletal muscle force estimation and LQG control algorithms for smart upper extremity prostheses

Chandrasekhar Potluri *, Madhavi Anugolu, D. Subbaram Naidu, Marco P. Schoen, Steve C. Chiu

Measurement and Control Engineering Research Center, Idaho State University, Pocatello, ID 83209, USA

ABSTRACT

This paper presents a real-time embedded framework for finger force control of upper extremity prostheses. The proposed system is based on the hypothesis that models describing the finger force and surface Electromyographic (sEMG) signal relationships of healthy subjects can be applied to amputees. An identification/estimation scheme is applied to the collected sEMG and finger force signals in order to infer dynamical models relating the two. A LQG control law is proposed based on this estimation scheme in order to control finger forces of upper extremity prostheses. For the force estimation, filtered sEMG signals from a sensor array and finger force data of a healthy subject are acquired. Real-time estimation and control are implemented using a PIC32MX360F512L microcontroller. In this paper, a novel fusion technique, the Optimized Linear Model Fusion Algorithm (OLMFA) is developed for estimating the skeletal muscle force from the sEMG sensor array in real-time. The sEMG signal is rectified and filtered using a Half-Gaussian filter, and fed to the OLMFA based Multiple Input Single Output (MISO) force model. This MISO system provides the estimated finger force as reference input to the upper extremity prostheses in real-time. A LQG controller is designed to control the finger force of the prostheses utilizing the force estimate from the OLMFA as a reference. Both the OLMFA and the LQG control scheme are prototyped on the embedded framework for testing of the real-time performance. The proposed embedded framework features rate partitioning and UART interface for performance validation and troubleshooting. The OLMFA based force estimation yields a real-time performance of 85.6% mean correlation and 20.4% mean relative error with a standard deviation of ± 1.6 and ± 1.5 respectively for 18 test subject's k-fold cross validation data. The LQG control algorithm yields a real-time performance of 91.6% mean correlation and 9.2% mean relative error with a standard deviation of ± 1.4 and ± 1.3 respectively.

© 2015 Elsevier Ltd. All rights reserved.

1. Introduction

According to the information provided by the National Limb Loss Information Center (Aca News: National Limb Loss Awareness

Month, 2011), the number of people with missing limbs in the United States is over 1.7 million due to combat and non-combat manoeuvres. The recent wars in Afghanistan and Iraq substantially increased the number of amputees; "at least 251,102 people have been killed and 532, 715 people have been seriously wounded" (Causalities in Afghanistan & Iraq, 2006). About 57% of them are trans-radial amputees (Causalities in Afghanistan & Iraq, 2006; Ziegler-Graham et al., 2008; Esquenazi and Meire, 1996; Merrill et al., 2011), about 80% of amputees use prosthetic devices (Biddiss and Chau, 2007) and around 30–50% of amputees are using myoelectric controlled devices (Kyberd and Hill, 2011).

Research in the field of prosthetic limbs was initiated in response to casualties during World War II by the United States National Academy of Sciences (Clynes and Milsum, 1970). The first EMG based control was developed by Wiener (1948). Advancements in the processors used in the prostheses have led to remarkable progress in nonindustrial robotics such as developing prosthetic devices for individuals who have sustained hand amputation. In nonindustrial robotics,

Nomenclature

A_1	mother chromosome
A_2	father chromosome
$B(q)$ and $F(q)$	polynomials
B_{wk}	matrix associated with the plant noise w_k of $n \times n$ dimension
F_f	fitness function
F_k	system matrix of $n \times n$ dimension
F_{kf}	$n \times n$ positive semi-definite matrix
$F_0(t)$	controlled force output
$G(q)$	transfer function providing the dynamic relationship
G_k	control matrix of $n \times r$ dimension
H	highest number in parameter range
$H(s)$	MISO transfer function
H_k	output matrix of $p \times n$ dimension
J	cost function
L	lowest number in parameter range
l	percentage load on the PIC
M_1, M_2 and M_3	estimated models from the sEMG sensor data $u_1(t)$, $u_2(t)$ and $u_3(t)$—and the corresponding skeletal muscle force
M_R	mutation rate
N_{IP}	population size of generations
N_{PA}	number of sensors
N_{PM}	number of parameters to be mutated
P_{ek}	$n \times n$ state estimation covariance error matrix
Q_k and R_k	covariance matrices associated with plant noise w_k and measurement noise v_k respectively.
T_{NP}	total number of parameters
$Y(t)$	skeletal muscle force
$\hat{Y}_f$	fused force output
$\hat{Y}_i$	estimated force
b, f	coefficients
$e(t)$	error
f, h	nonlinear functions
g_i	low-pass filter with impulse response
h_i	high pass filter
h_j	individual's cumulative probability
i	corresponding sensor
n	number of data points
n_k	system delay
nb, nf	row vectors
os_1, os_2	off springs
p_i	order of particular model
$p_1, p_2, \dots, p_N$	chromosomes
p_d	PWM wave with specific duty cycle
$\tilde{p}_j$	jth probability to be selected.
q	back shift operator
u_k	selected control strategy
t	time index
t_0, t_f	initial and final time
u_k	control vector of r dimension
v_k	measurement noise of p dimension
x	latent driving signal
x_k	state vector of n-dimension at any instant k
x_{kf}	$n \times n$ state vector at final instant kf
y_k	output vector of p dimension
α	expected rate of gradual drift
β	expected rate of sudden shift in the signal
β_{GA}	random number on the interval [0, 1]
λ, υ	weighing coefficients
μ	steady state population
ϑ	is the proportion of a generation population kept for the mating process
$|sEMG|$	rectified EMG signal

'rehabilitation robotics' has been an active research area for the past two decades. Rehabilitation robotics is human-centered and addresses a different set of requirements such as mechanical compliance, flexibility, adaptability towards the user, gentleness, safety and, last but not least, humanoid appearance and behavior (Zinn et al., 2004). Past research stipulates that human-centered robotics must be autonomous with a high level of functionality, pleasure, comfort and ease of use (Bien and stefanoy, 2004). One interesting domain of rehabilitation robotics is human-machine interface. Human-centered robotics requires a natural means of communication (Heinzmann and Zelinsky, 1999) and, in the case of EMG based prostheses, one natural means of interface between the human arm and prosthesis is the surface Electromyographic (sEMG) signal itself. The sEMG signals are electrical voltages ranging less than 50 μV and up to 20–30 mV (Raez et al., 2006). The sEMG signals are always available when sufficient muscle tissue exists. The signal's strength and variability depends on different movements and force levels. sEMG signals are acquired using suitable sensors and are used as an input to the control scheme of the hand prostheses in order to control the movements and forces applied by the prosthetic fingers. As sEMG signals are collected from the surface of the skin, the signals pass through numerous tissue layers before they reach the skin surface where they can be acquired by the EMG sensors (Cram et al., 1998). Hence, the signals are prone to cross-talk, interference and noise. For this work these EMG signals are acquired using a Delsys Bagnoli-16 system. The acquired signals are rectified and filtered using Half-Gaussian filter before estimating the sEMG–force relationship.

To date there are many commercial prostheses available. A few to name are: the Utah arm 3 from Motion Control (Motion Control, Salt Lake City, UT, 2011), Myolino wrist by Otto Bock (Otto Bock Duderstadt, 2011), Bebionic V2 from RSL Steeper (RSL Steeper Leeds, U.K., 2011), Shanghai Kesheng (Shanghai Kesheng Prostheses, 2011), iLimb from Touch Bionics (2011), and the Boston elbow by Liberating Technologies Holliston, MA (2011). The Boston elbow prosthesis has one degree of freedom i.e., elbow flexion. It evaluates the subject to determine the muscle groups and experiments with various control strategies until the appropriate one is found (Toledo et al., 2009). A Motion Control Hand uses a simple proportional controller based on the slope of the normal feedback force to provide a more natural feeling based control for hand prosthesis and to avoid force overshoot (Fougner et al., 2012). The Otto Bock hand uses a three dimensional force feedback in order to give the directly proportional relationship between the applied force and user's input (Puchhammer, 2000). The unique feature of the iLimb is given by the ability to add additional force to the object. However, there are some limitations; for example, heavy tasks execution is impossible because of the limited power provided by the iLimb. Most of the commercially available prostheses have predefined gestures/grasping actions which utilizes real-time classifiers. According to Kaveh et al. (2007) there are very few real-time classifiers available in the literature which can be utilized towards hand gesture classification. In Nishikawa et al. (2001) an adaptive heuristic critic (AHC) real-time algorithm was proposed for predefined hand movements. Using wavelet analysis, a continuous classifier was developed for steady-state EMG signals (Englehart et al., 2001). A real-time pattern recognition algorithm based on K-nearest neighbors was proposed in Christian et al. (2011). It concludes that using EMG patterns, hand gestures can be decoded in real-time and can control an artificial hand.

The use of real-time classification algorithm cannot detect the small changes in the sEMG and react to fine finger force control. Past research indicates that the typical approach to the control of a prosthetic hand is to use a data driven sEMG force estimation combined with the hybrid position and force control (Railbert and Craig, 1981). There are several interpretations of the sEMG–force relationship. The sEMG–force estimation research has been ongoing since the 1950s (Schwartz, 2012). A very common and standard method for sEMG–force estimation is adopting a Hill model which utilizes Vander Waals equation (Mitsuhiro and David, 2013). The main drawback of the Hill model is that the estimation errors will be large at different firing frequencies, levels of activation, and speed of muscle contraction. Another common approach (Mitsuhiro and David, 2013; Istenic et al., 2007) to the sEMG–force estimation problem is using a physiological model achieved by combining a motor unit twitch model with motor unit pulse trains obtained from the multi-channel sEMG.

In the present work, a data driven methodology based on system identification (SI) is investigated. In particular, a linear Output Error (OE) model for the sEMG–skeletal muscle force estimation problem is adopted. We also utilized an array of sensors and developed a Genetic algorithm based Optimized Linear Model Fusion Algorithm (OLMFA) for the better estimation of skeletal muscle force from the corresponding sEMG signals of the sensor array. This kind of a data driven approach provides better EMG/skeletal muscle force estimation when compared to real-time classifiers even for smaller muscular contractions. Therefore, skeletal muscle force estimation based on the sEMG data is utilized as reference force profile for the prostheses finger force control. A real-time embedded test bed and an intelligent control system is essential for this design to accomplish its goals. Such a control system combines hardware and software components to balance the computational, electrical and mechanical workloads across the system.

The proposed work utilizes a discrete time Linear Quadratic Gaussian (LQG) controller, a combination of the Linear-Quadratic Estimator (LQE) and Linear-Quadratic Regulator (LQR), and is implemented on an embedded framework to control the movements and force of a prosthetic hand prototype with force feedback to the controller. The LQE (Kalman filter) is used extensively in biomedical applications that involve non-linear dynamic models for noise-corrupted measurements which need to be monitored and controlled continuously, because it produces output values close to the true values of the measurement (Widjaja et al., 2008). For instance, a Kalman filter is used for filtering the noisy Electro Cardiogram (ECG) signal (Sameni et al., 2005) to remove environmental noise and artifacts from the signal. A two-stage Kalman filter, i.e. an LQG scheme, is designed for estimation and control of real-time human body motions (Kwang-Hoon et al., 2008; Xiaoping and Eric, 2006). In this paper we proposed a LQG control scheme along with an embedded framework for the real-time state estimation and control the force of a prosthetic hand. The input to the real-time control system is a fusion-based force estimate. A two-stage embedded

framework design with an LQG controller is chosen for the force control of the prosthetic hand prototype. The proposed LQG control strategy is a semi-autonomous control system which maintains the estimated skeletal muscle force from the fusion algorithm, with the help of the prosthetic hand fingers, even without a bio feedback. Since the proposed control strategy has a fine force control, it can grasp irregular and sensitive objects with ease. This paper also details the embedded framework for real-time estimation and control of the finger force based on the sEMG signals. The block diagram in Fig. 1 gives a brief insight into the paper outline.

A detailed comparison of the fusion algorithm based LQG, Model Reference Adaptive Control (MRAC) (based on MIT rule) (Karl and Bjorn, 2008) schemes and the performance of the embedded framework in terms of correlation accuracy and the percentage load on the microcontroller for 18 test subjects are presented in this paper. In addition, the fusion algorithm is compared with the existing literature (Lopez et al., 2009) Variance Weighted Average (VWA) and Decentralized Kalman Filter (DKF) based data fusion algorithms. LQG control strategy and the embedded framework design are also compared with state of the art existing work, such as adaptive heuristic critic (AHC) real-time algorithm and a real-time K-nearest neighbor's pattern recognition algorithm (Nishikawa et al., 2001; Englehart et al., 2001; Christian et al., 2011).

A non real-time version of the proposed fusion algorithm is presented in Potluri et al. (2010). A simulation based (non-real-time) Linear Quadratic Regulator (LQR) is schemed for the finger force control and tested on a mathematical model of the hand (not the real prosthetic hand) (Potluri et al., 2011). The authors utilized their previous work (Potluri et al., 2010, 2011) as a proof of concept before implementing concepts real-time. The main objective of the presented work is to create a real-time embedded framework for the fusion algorithm and LQG control scheme for rigorous real-time performance testing based on 18 different subject's k-fold cross validation data. Therefore, the embedded framework will achieve the following rapid prototyping requirements for the prosthetic hand technology development.

1. It should be able to accurately estimate and control skeletal muscle force based on the sEMG data of the subjects.
2. The estimation and control of the skeletal muscle force has to be achieved in real-time. Therefore all the computation should be performed without any over-run's with a reasonable load on the micro-processor.

2. Experimental set-up

The experimental set-up used to acquire the sEMG and its corresponding skeletal muscle force signals is as shown in Fig. 2. The experiments were conducted on 18 healthy subjects (mean age of 27.3 years, Standard Deviation (SD) of 2.1; 5 women and 13 men). The subject's skin surface is prepared in accordance with the
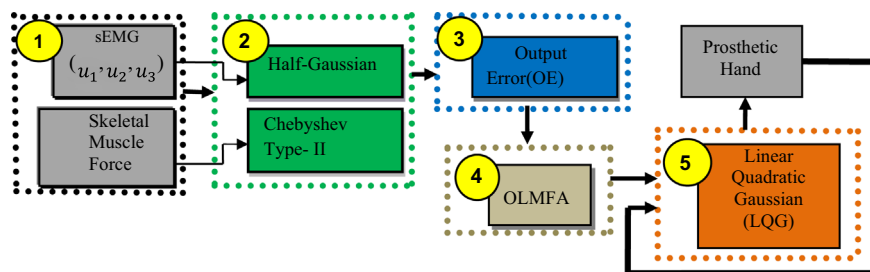

Fig. 1. Block diagram representation of overall proposed scheme. Data acquisition block represents the acquisition of the sEMG and the skeletal muscle force signals. The signal preprocessing block represents the various filtering techniques used in this work. The system identification (SI), the data fusion algorithm and the Controller blocks represent the SI techniques, the data fusion and control algorithms employed in this work. (1.) Data Acquisition (2.) Signal Processing/Filtration (3.) System Identification (4.) Data Fusion (5.) Controller
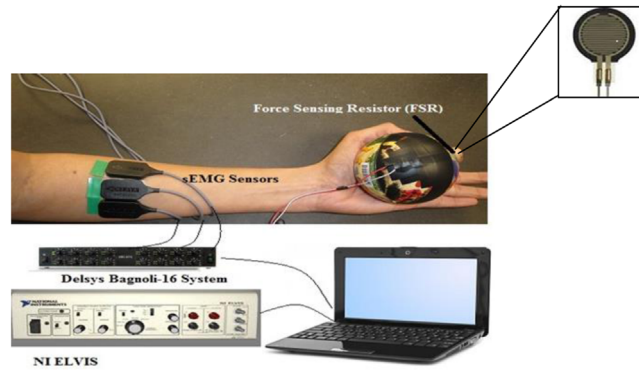
Fig. 2. Experimental design for sEMG and the skeletal muscle force acquisition.
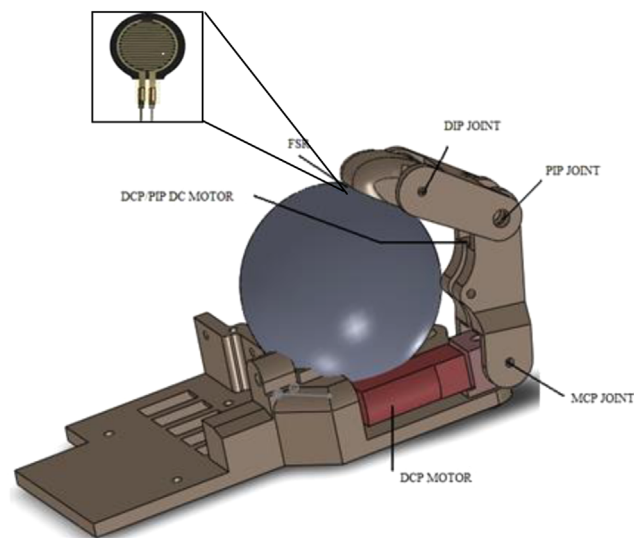

Fig. 3. Actuation scheme for the prototype finger.

International Society of Electrophysiology and Kinesiology (ISEK) protocols (Merletti, 1999). Using a muscle point stimulator (Rich-Mar Corporation, model number HV 1100), the motor point locations of the Flexor Digitorum Superficialis (FDS) and the appropriate EMG electrode attachment points of the subjects were identified. The forearm of each subject's dominant hand is used. The Flexor Digitorum Profundus (FDP) is also involved in the action of finger flexion, but it lies deeper than the FDS and hence the sEMG capturing includes both muscles in the finger motion. During the data acquisition, each subject is requested to keep the wrist at neutral position and flex only the index finger while keeping fingers III–V stationary. Three sEMG sensors are mounted on the skin surface of the test subject's dominant hand as shown in the figure. One sEMG sensor is placed on the motor point and the other two sensors are placed adjacent to the motor point at a distance of 1.5 cm on either side of the sensor on the motor point.

A Delsys®, Bagnoli-16 channel EMG, DS-160, S/N-1116 system is used to capture the EMG data from the skin surface. This data acquisition system has an internal amplification gain of 1000 and a bandwidth of 20–450 Hz and line voltage isolation of 6000 VDC, 4200 VAC (RMS). The sEMG signals are acquired by mounting pronged DE 2.1 differential surface electrodes and a reference electrode on the subject's elbow (⟨http://www.delsys.com/Products/Bagnoli_Desktop.html⟩). A model 402 single zone Force Sensitive Resistor (FSR) optimized for human touch control of electronic devices is used to obtain the finger contact force from each finger. It has a 46.7 mm^2 active diameter area with a force sensitivity range of 0.1–100 N, force repeatability of $\pm 6\%$ and a

continuous force resolution (Interlink Electronics). During data acquisition each subject is requested to perform a random grasping action (index finger flexion and extension) for duration of 9–10 s with a moderate force production to avoid fatigue using a stress ball for added resistance. While doing so, the random grasping action finger force is applied on the FSR, which is mounted on the stress ball by the index finger distal phalanx. Both the sEMG and the corresponding skeletal muscle force are acquired simultaneously using NI LabVIEW™ with a single data acquisition board (DAQ NI 6024E) at a sampling rate of 2000 Hz. Since the content of the sEMG signal is in the range of 20–450 Hz, the sampling rate is set at more than twice the range of the Nyquist frequency.

For the implementation of the proposed control and estimation scheme, a simple prosthetic hand prototype is used that has one controllable finger, as shown in Fig. 3. The prosthetic hand prototype finger has three degrees of freedom and is actuated by two Pololu 35:1 mini metal gear motors and a bevel gear transmission system. The main characteristic of this prosthetic prototype is its biologically inspired parallel actuation system, which is based on the behavior/strength space of the Flexor Digitorum Profundus (FDP) and the Flexor Digitorum Superficialis (FDS) muscles (Anthony et al., 2010).

Fig. 3 shows the actuation scheme of the prototype finger. The DC motor in the proximal phalanx of the finger actuates the Proximal Inter Phalangeal (PIP) joint and through the belt transmission system, the motor also drives the Distal Inter Phalangeal joint DIP. The DC motor at the metacarpus actuates the Meta Carpo Phalangeal (MCP) joint.

3. Methodology

The main objective of the two-stage embedded control scheme is to track the estimated force signal as closely as possible for the prosthetic hand finger. In this work, the force signal is deduced from sEMG signals obtained from the array of the three sEMG sensors located at the arm. The sensor fusion algorithm (OLMFA) is used to provide the best finger force estimation from the pre-processed sEMG data. Using a simple elitism based genetic algorithm (GA), sensor fusion is achieved for the sEMG data.

3.1. Filtration

The sEMG data from the three sensors are collected around each corresponding individual motor point at the trans-radial arm location (Flexor Digitorum Superficialis). As the motor point location is approximated for the sEMG sensor placement, the sEMG sensor picks up a significant portion of EMG from the motor point. The data is rectified and filtered using a Half-Gaussian filter before being fed into the fusion algorithm to eliminate the cross-talk (Anugolu et al., 2009). Cross-talk exists due to the simultaneous firing of different motor points. The half-Gaussian filter is given as follows:

$$P(\text{sEMG}|x) = 2 \times \frac{\exp\left(-\text{sEMG}^2/2x^2\right)}{\sqrt{2\pi x^2}} \tag{1}$$

where $P(\text{sEMG}|x)$ is a conditional probability density function, x is the latent driving signal representing group delay, which is used to compute the conditional probability of the filter and sEMG is an input signal. The skeletal muscle force is filtered by a low-pass Chebyshev type II filter with a cut-off frequency of 550 Hz according to the ISEK standards (Merletti, 1999).

3.2. System identification (SI)

The identification of the dynamical relationship between the sEMG data from the three sensors $u_1(t)$, $u_2(t)$, $u_3(t)$ and the corresponding finger contact force $Y(t)$ of a healthy subject is achieved by employing a system identification (SI) technique. In this fusion algorithm, Output Error (OE) models are used and are constructed for the data coming from each individual sEMG sensor and its corresponding skeletal muscle force. The general OE model structure is given as follows:

$$y(t) = \frac{B(q)}{F(q)}u(t - nk) + e(t) \tag{2}$$

where $B(q)$ and $F(q)$ are the polynomials, q is the back shift operator, $e(t)$ is output error, $y(t)$ is system output, u is input, nk is the system delay, and t is the time index.

3.3. Optimized linear model fusion algorithm (OLMFA)

To develop the OLMFA, a GA is utilized. The GA has the objective to find the optimum values for a transfer function which is defining the input (sEMG) and estimated output (force). In particular, the transfer function's numerator is optimized. As this is a multi-input system (sEMG sensor array), there are multiple numerators (as many as sensors). Each numerator is optimized by finding the optimum zeros of the numerator polynomial. The denominators are given by the results of the system identification.

The steps of the GA include the initialization of the chromosomes (detailed in Step 2 below). Here, chromosomes are defined as the set of parameters that make out a feasible solution. Using a cost function, a chromosome can be evaluated and assigned a fitness value. This fitness value is used in the selection operation of the GA (step 4). After the selection of parent chromosomes, a mating operation creates offspring. The offspring undergo a mutation operation, where a small set of genes are mutated. The GA repeats itself by using the cost function and assigning fitness values for the next generation.

The following fusion technique is applied to the sEMG–force identification model:

Step 1: Considering the sEMG data $u(t)$ as input and force data $Y(t)$ as output, the sEMG/force linear Models $M_1(s)$, $M_2(s)$, ..., $M_n(s)$ are identified using regular linear system identification. Each model is of the structure as given by Eq. (2). Here, s is the complex variable $s = \sigma + j\omega$, which can be substituted for the q operator in Eq. (2).

Step 2: A hybrid transfer function $H(z)$ is constructed by utilizing the denominators of the identified models $M_1(s)$, $M_2(s), ..., M_n(s)$ and numerators as defined by: $C = [p_1, p_2, ..., p_N]$, is the chromosome, and $p_1, p_2, ..., p_N$, are the genes. Each gene represents a zero of the numerator polynomial of the transfer function. The value of these genes is established in Step 3.

Step 3: Initial population (IP) is computed by

$$IP = (H - L)^* R_N + L,$$

where H is the upper limit of each of the parameters p_i (gene), L is the lower limit of the parameters p_i. H and L define the search area for each parameter, R_N is the random number $\{N_{IP} - N_{PA}\}$, N_{IP} is the population size of generations and N_{PA} is the number of sensors.

Step 4: Selection: selecting two chromosomes as the parent chromosomes in order to create two offspring. The selection is based on the fitness function (see Step 8), where each chromosome gets a probability assigned of being selected as a mate. The probability is based (proportional) to the fitness ranking among all other chromosomes within the population. Considering one chromosome being selected based on the linear rank algorithm, the associated probability density function can then be given as

$$\tilde{p}_j = \frac{J(C_j)}{\sum\limits_{i=1}^{\text{repl}} J(C_i)},$$

where J is the cost function, and $\tilde{p}_j$ is the jth probability to be selected. The number of replacement chromosomes chosen is determined by repl $= 0.5*(\mu - \vartheta)$, where μ is the steady state population—the population which will be maintained for the duration of the algorithm, with the exception for the first generation, which usually has a larger size of chromosomes. ϑ is the proportion of a generation population kept for the mating process. The selection of the chromosome is accomplished by using the individual's cumulative probability

$$h_j = \sum_{k=1}^{j} \tilde{p}_k, \quad \text{if} \quad \rho_j(0,1) < h_j \quad \text{and} \quad \rho_j(0,1) > h_{j-1},$$
$$\text{then} \quad C_{\text{MotherorDad}} = C_j \quad \text{else} \quad C_{\text{MotherorDad}} = C_1.$$

Here $\rho(0,1)$ represents a uniformly distributed random variable between 0 and 1.

Step 5: Mating: The mating operation follows a similar approach to the binary implementation of GA where a cross-over point is selected and the chromosome is partitioned and exchanged the complementary part of another selected chromosome:

$$\alpha_{GA} - \text{Roundup}\{N_{PA}\}, \quad C_1 = [a_{m_1}, a_{m_2}, ..., a_{m_\alpha}, ..., a_{m_N}],$$
$$C_2 = [a_{d_1}, a_{d_2}, ..., a_{d_\alpha}, ..., a_{d_N}]$$

a_{m_N} is the nth parameter in the mother chromosome, a_{d_N} is the nth parameter in the father chromosome.
Then

$$C_{new1} = a_{m_\alpha} - \beta_{GA}[a_{m_\alpha} - a_{d_\alpha}], \quad C_{new2} = a_{d_\alpha} + \beta_{GA}[a_{m_\alpha} - a_{d_\alpha}]$$

β_{GA} is the random number on the interval [0,1].
Then the offspring's or new chromosomes are found as

$$os_1 = [a_{m_1}, a_{m_2}, ..., a_{new_1}, ..., a_{d_N}], \quad os_2 = [a_{d_1}, a_{d_2}, ..., a_{new_2}, ..., a_{m_N}],$$

where os_1, os_2 are the off spring.
Step 6: Mutation: The mutation is accomplished by randomly change some of the parameters within the off spring chromosomes. The number of mutations is given by the mutation rate.

$$M_R{}^* T_{NP} = T_{PM}$$

where M_R is the mutation rate, T_{NP} is the total number of parameters, N_{PM} is the number of parameters to be mutated.
Step 7: Compute the cost of each chromosome using

$$J = \lambda \sum_{i=1}^{n} \left| Y(t-i) - \hat{Y}_f(t-i) \right|^2 + \nu \left(corr\left[Y, \hat{Y}_f \right] \right)$$

where λ and ν are weighting coefficients and 'corr' is the correlation function.
Step 8: The Fitness function, F_f, is computed by

$$F_f = \int_{t_0}^{t_f} \left(\hat{Y}(t) - Y(t) \right)^2 dt = \int_{t_0}^{t_f} \phi^2(t)dt.$$

where t_0 and t_f are the initial and final time values, $\hat{Y}(t)$ is the fusion model estimated force and $Y(t)$ is the actual force from the FSR
Step 9: The objective function is set as the error squared of the resulting MISO system. The discrete time transfer function $H(z)$ is then given as

$$H(z) = \begin{pmatrix} \frac{A_{1,1}z^n + A_{1,2}z^{n-1} + \cdots + A_{1,n+1}}{B_{1,1}z^n + B_{1,2}z^{n-1} + \cdots + B_{1,n+1}} \\ \frac{A_{2,1}z^n + A_{2,2}z^{n-1} + \cdots + A_{2,n+1}}{B_{2,1}z^n + B_{2,2}z^{n-1} + \cdots + B_{2,n+1}} \\ \frac{A_{3,1}z^n + A_{3,2}z^{n-1} + \cdots + A_{3,n+1}}{B_{3,1}z^n + B_{3,2}z^{n-1} + \cdots + B_{3,n+1}} \end{pmatrix}$$

where A's and B's are the numerator and the denominator coefficients respectively of the individual transfer function and n is the order of the system. The A's are computed from the optimum zeros in C. The OE model computed of order (n) for the sEMG/skeletal muscle force linear system is eight (see the Appendix).
Step 10: Feeding new data sets to the Multiple Input Single Output (MISO) transfer function $H(z)$ will result in an estimated OLMFA based force $\hat{Y}(t)$.
Based on the poles of the three linear models, corresponding to each sensor, a Multiple Input Single Output (MISO) transfer function $H(z)$ is constructed. While the denominators of the respective individual transfer functions (corresponding to each OE model) are superimposed on the new MISO transfer function, the corresponding zeros are found using GA. Generally GA's can find global optimum points if an elitism scheme is used and a sufficient number of generations are allowed in the algorithm (Schoen, 2008). In this work $H(z)$ is constructed from single subject data and cross validated with the rest of the subjects. It is computed offline by using the system identification and the GA to find its optimal zeros as part of the proposed OLMFA algorithm. This optimization algorithm is rather computationally expensive, however since this can be done offline, there was no computational time requirement, and one is free to use GA rather than other intelligence based algorithms.

Chromosomes are constructed by designating each zero of a numerator as a gene. Since a discrete time model is utilized, the search area is limited to the unit circle and the resulting MISO model is decreased to be in minimum phase. The number of potential zeros was set to the order of the corresponding denominator. MISO transfer function model validation is done by k-fold cross validation to test the accuracy of the predictive model $H(z)$. The following parameters were used for the employed GA: Maximum Number of iterations: 100; Population Size of Generation: 48; Population Size for Generations: 24; Number of Chromosomes kept for mating: 12; Total Number of parameters in a chromosome: 1; Mutation rate: 0.04; High end of parameter value: 1; Low end of parameter value: 0.

3.4. LQG controller design

During the development of the artificial hand, changes were undertaken to the mechanical design and drive trains of the hand that affect the dynamics of the prosthesis finger motion. In addition, the uncertain characteristics of kinematic and actuator interaction may lead to different performance than expected. Hence, an LQG controller is utilized in order to maintain performance stability. The simplified block diagram of the LQG controller is given in Fig. 4.

The LQG controller is designed to compensate for the process (mechanical design) and the measurement (force sensor) noise of the skeletal muscle force and achieve a desired real-time performance. The LQG controller is a well-established concept, for which the stability issue has already been addressed in literature (Naidu and Chen, 2011).

The LQG control algorithm with its computational expense is given as follows:

Given the prosthetic hand model (Naidu, 2002),

$$x_{k+1} = F_k x_k + G_k u_k + B_{wk} w_k \tag{3}$$

where x_k is a torque (state) vector of n-dimension at any instant k which is derived from the skeletal muscle force (Potluri et al., 2011), F_k is the system matrix of $n \times n$ dimension, G_k is the control matrix of $n \times r$ dimension, u_k is the fusion algorithm based scaled sEMG–force (torque) signal (control vector) of r dimension, B_{wk} is the matrix associated with the plant noise w_k of $n \times n$ dimension.

The measurement is

$$y_k = H_k x_k + v_k \tag{4}$$

where y_k is the skeletal muscle force output vector of p dimension, H_k is the output matrix of $p \times n$ dimension, v_k is the measurement noise of p dimension and k represents discrete time index with conditions as

$$\varepsilon\{w_k w_k'\} = Q_k, \ i = k, \ \text{and} \ 0, i \neq k$$

$$\varepsilon\{v_k v_k'\} = R_k, \ i = k \ \text{and} \ 0, i \neq k,$$

$$\varepsilon\{w_k w_k'\} = 0 \forall \ i \ \text{and} \ k$$

Q_k and R_k are covariance matrices associated with plant noise w_k and measurement noise v_k respectively.

The performance index is chosen as

$$J(x_{k_0}, k_0) = \varepsilon \left\{ \begin{array}{l} \frac{1}{2} x_{kf}' F_{kf} x_{kf} + \\ \frac{1}{2} \sum_{k=k_0}^{k_f - 1} [x_k' Q_k x_k + u_k' R_k u_k] \end{array} \right\} \tag{5}$$

x_{kf} is the $n \times n$ state vector at final instant kf, F_{kf} is the $n \times n$ positive semi-definite matrix. Using Q_k and R_k in Eq. (5), the Kalman gain K is computed (see Naidu, 2002 for details) und used for the proposed LQG controller implementation.
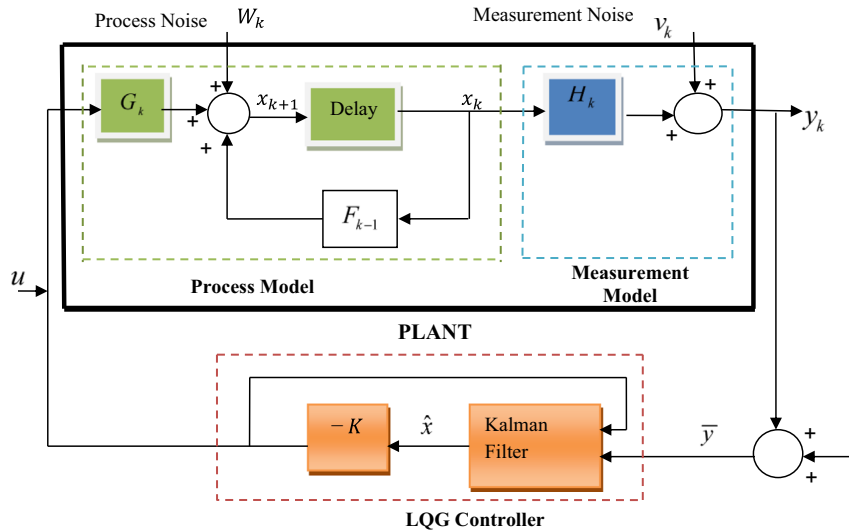
Fig. 4. LQG control scheme for the prosthetic hand, with the process and the measurement models and their corresponding noises and the LQG controller for both the estimation and the control.
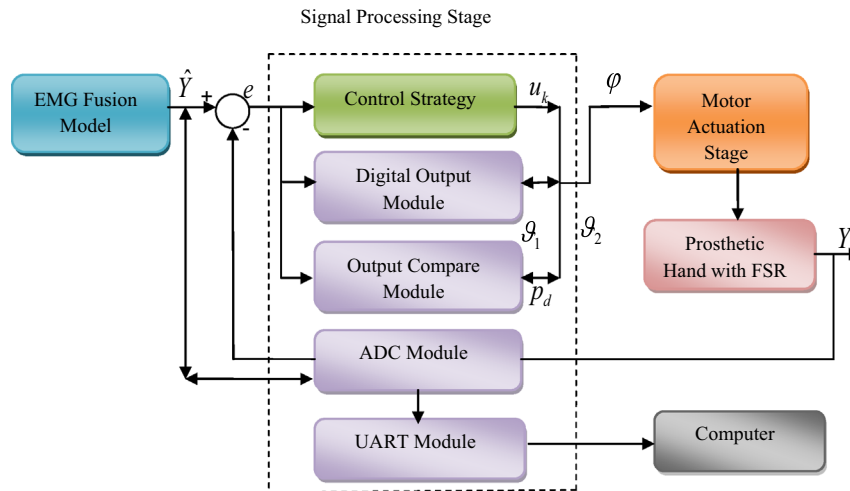

Fig. 5. Block diagram representation of real-time embedded framework with the signal processing and motor actuation stages.

4. Real-time implementation of the proposed fusion and LQG algorithms

Skeletal muscle force is estimated from the measured sEMG data in real-time utilizing the established transfer function $H(z)$. The real time force data is used along with the proposed LQG controller to achieve, real-time finger force control of the prosthesis. The force feedback signal for the controller is acquired by an FSR, which is mounted at the fingertip of the prosthetic hand prototype. The error $e(t)$ is computed as the difference between the OLMFA estimated force and the actual force from the force sensor.

To impose a desired dynamical response, an LQG controller is designed to track the actual force from the force sensor, equating it to the OLMFA force estimate (reference force profile), and to minimize the error $e(t)$. The fast prototyping of the above methodology is achieved by an embedded framework using a PIC 32MX360F512L microcontroller. A block diagram of the real-time embedded framework is given in Fig. 5.

The real-time embedded framework is designed as a master-slave configuration "Signal Processing" and "Motor Control Logic".

The Signal Processing stage facilitates the skeletal muscle force estimation and control and acts as the master configuration. The dsPIC block set tool chain is used to generate the 'Assembly C' code for the target device (i.e. the PIC 32MX360F512L) from Simulink™. In order to optimize the micro-controller CPU utilization rate partitioning is done at the signal processing stage. All analog and the digital I/O are running at 2000 Hz, i.e. 0.0005 time steps.

The fusion algorithm for the sEMG/skeletal muscle force estimation and the LQG controller are running at 4000 Hz i.e. 0.00025 time steps. The skeletal muscle force estimation and the LQG control are running at twice the rate of the I/O's. The up-sampling of I/O's is achieved by Local Over Sampling (LOS) utilizing a low pass first order digital filter with a First Order Hold (FOH). The phase lag caused by the filter and the FOH is corrected by utilizing a feedback loop with a proportional gain of 10.64 at every 0.0005 time step. Fig. 6. shows the LOS block diagram, where $x[n]$ is the input data array for the LOS block, $y(k)$ is the signal from the low pass first order digital filter with a FOH, FS_{in} and FS_{out} are the fudge parameter gain of the LOS block and $y[m]$ is the up-sampled output data array. In this figure, n, k and m show different time instances of the finger force signal due to LOS.
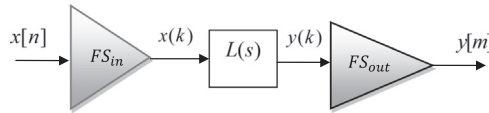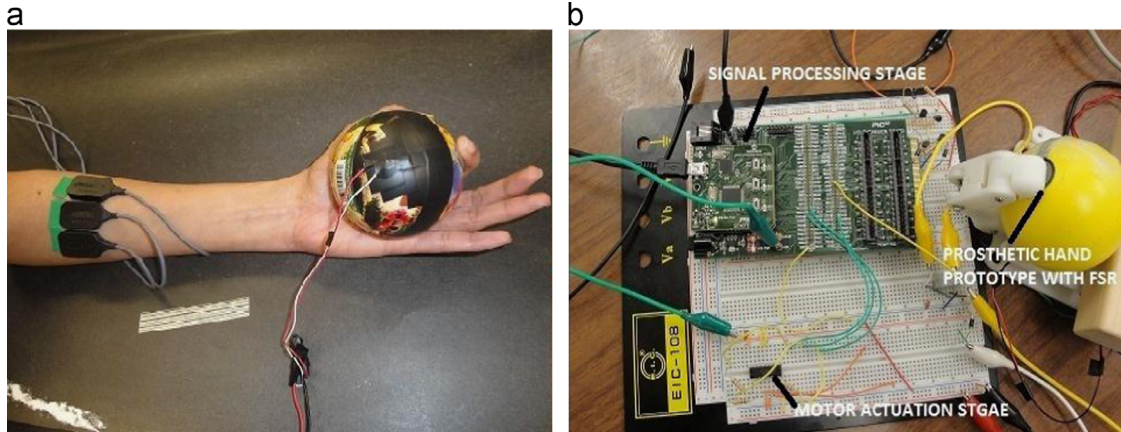
Fig. 6. Up sampling block structure.

Fig. 7. (a) sEMG and skeletal muscle force real-time acquisition 7. (b) Embedded test platform for prototyping the fusion algorithm and the LQG control scheme.

4.1. Signal processing stage

The acquisition of finger force feedback data from the FSR is accomplished by the PIC's internal analog to digital converter (ADC) module. The internal ADC of the PIC 32 has a 10-bits precision, yielding 3 mV resolution. The FSR (finger force) data is also acquired at 2000 samples/s by the PIC 32 to match the offline sEMG/skeletal muscle force sampling rate. The Digital Output module is used to generate control signals, based on the LQG control strategy (u_k) and transmit them to the motor actuation (slave) configuration. This module detects the changes in the reference/command signal and flips the direction bits (ϑ_1, ϑ_2) between 0 and 1, facilitating the grasping/actuation action of the prosthetic hand prototype. Depending on the error $e(t)$ a Pulse Width Modulated (PWM) wave with a specific duty cycle (p_d) is generated by the Output Compare module to adjust the speed of the grasping action. The mathematical representation of the signal processing stage is given as

$$\varphi = u_k p_d e(t)\{\pm \vartheta_1 \pm \vartheta_2\} \qquad (6)$$

The UART module of the PIC32 is used to transmit the FSR (finger force) data from the PIC32 to the PC via serial communication through a serial virtual COM port, facilitating on-chip debugging and monitoring. This real-time communication link of the embedded framework enables performance and accuracy evaluation of the control strategy.

4.2. Motor control logic

In this stage, a SN754410 quadruple half-H driver (Texas Instruments, 1995) is used to actuate the motors with the corresponding control signal. The PWM wave from the Output Compare module is transmitted to the enable pin of the H driver. The PWM wave (p_d) which is a function of error $e(t)$ enables this H driver and controls the grasping action speed by varying the duty cycle of the PWM wave. Therefore grasping action speed is adjusted based on error to achieve desired performance and accuracy. The digital outputs (ϑ_1, ϑ_2) of the PIC32 are transmitted to the direction pins of the H driver. Switching the digital outputs (ϑ_1, ϑ_2) to 0 and 1 between the pins makes the fingers open and close. This rotation controls the finger to maintain the force levels based on the control strategy and reference signal. Therefore the finger force control, which is a function of torque at each joint,

is achieved by changing the position of the fingers. The motor control logic is the slave configuration for the signal processing stage. The communication between the master-slave configurations is achieved by Pulse Code Modulation (PCM) ϑ_1, ϑ_2 bits and a PWM wave (p_d).

The two stage real-time embedded control design is tested on an index finger of the prosthetic hand prototype. The force feedback data is acquired from the microcontroller through a secondary channel of the UART of the PIC32 by a virtual com port at 57,600 baud rate. The data is converted into unsigned 16 bit integers before it is transmitted through the UART. The target device (PIC32) is running at 80 million instructions per second (MIPS) with its Phase Lock Loop activated. It is running at an external clock frequency of 8 MHz with internal scaling and rate partitioning enabled to achieve 80 MIPS.

Fig. 7 shows the embedded test platform for the real-time acquisition of the sEMG signals and the implementation of the proposed control system design and the sEMG/skeletal muscle force fusion algorithm with a prosthetic hand prototype.

Fig. 8 shows the overall computational expense of the OLMFA sEMG/skeletal muscle force estimation, LQG controller, Up sampling and the motor control logic. The computational expense of the overall methodology from Fig. 8, is used to calculate the CPU utilization of the proposed embedded framework for the prostheses control applications. The CPU utilization and the robustness of the embedded framework are discussed in the results and discussion section. Quantitative analysis of the results is achieved by computing percentage correlation (ρ) and relative error (η) between the actual force ($Y(t)$) and the fusion algorithm estimated force ($\hat{Y}_f$).

5. Results and discussion

The results are presented in two sections in which the theoretical and experimental real-time performance of the controller as well as the two stage embedded design are evaluated.

5.1. Theoretical

The prosthetic hand index finger's mathematical model (i.e. Eq. (4)) (Ruoyin and Jiting, 2010) is used instead of the prosthetic hand prototype to obtain the controlled (simulation-based) force output
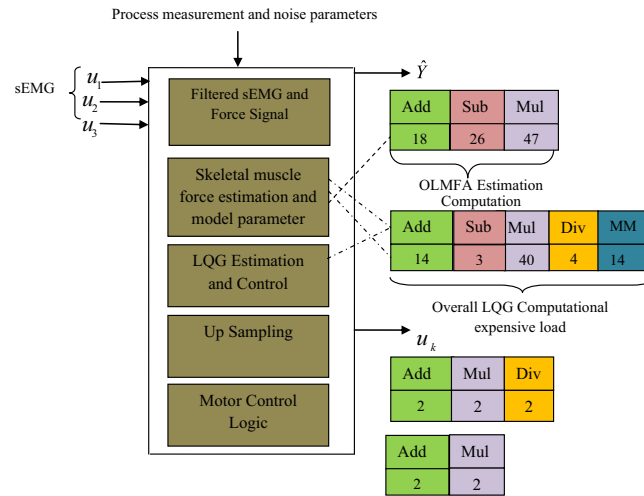
Fig. 8. Computational expense for the OLMFA estimation, LQG control, up-sampler and the motor control logic.
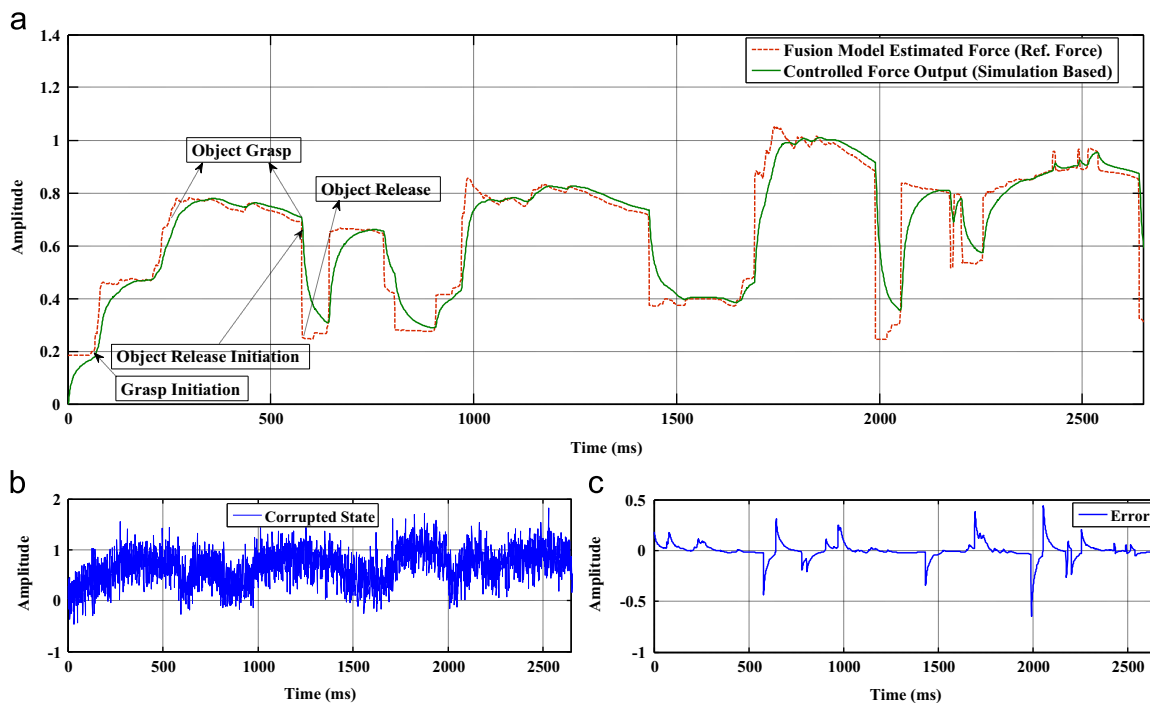

Fig. 9. Shows the non-real-time performance of LQG controller: (a) fusion-based force estimate and simulation-based force during the grasping action with time index on x-axis and force in Newtons on y-axis. (b) Band limited white noise corrupted signal state, (c) error between the model reference and the simulation based forces during the grasping action. (a) Simulation and Controlled Forces, (b) Controller State and (c) Error.

$F_0(t)$ and to validate the offline (non-real-time) controller performance. Fig. 9a shows the fusion model estimated skeletal muscle force $\hat{Y}$ and the force output from the controller $F_0(t)$. The controlled force output $F_0(t)$ approaches the fusion model estimated force $\hat{Y}$ in approximately 0.2 s. It is evident that the LQG controller can track the changes in the reference force profile, and follow those changes very closely after the convergence. Fig. 9a also demonstrates detailed grasping action: Grasp Initiation (GI), Object Grasp (OG), Object Release Initiation (ORI), and Object Release (OR). Fig. 10a shows the validation with a different reference force profile $\hat{Y}(t)$. To test the robustness of the proposed design all patterns are randomly chosen by the subjects and the index finger is extended maintaining the contact with the FSR.

In both cases, to test the performance and accuracy of the LQG controller, the signal is corrupted with a band limited white noise before it is fed into the controller. The corrupted input signals are shown in Figs. 9b and 10b. Even though the signals are corrupted

with noise, the LQG controller is able to track the reference force $\hat{Y}(t)$ effectively, as shown in Figs. 9a and 10a.

The tracking performance indicates that the controller can reduce the disturbances caused by the actuator gears, motors and other external factors to achieve the desired dynamic response. In both cases the Pearson correlation coefficient ($\rho_{x,y}$) (see the Appendix) for the reference force profile $\hat{Y}(t)$ and the controller output force $F_0(t)$ is 0.944 and 0.945, respectively. Figs. 9c and 10c show the error plot between the fusion-model estimated force $\hat{Y}(t)$ and the force output from the controller $F_0(t)$ for the two different result sets shown in Figs. 9a and 10a. These figures show that the error converged to zero in a very short time, and the error hovered near zero throughout the grasping time interval. The theoretical design is validated with 15 different data sets, and a mean correlation of 94% (0.9456) is achieved between the fusion model reference force $\hat{Y}(t)$ and the controlled (simulation based) force output $F_0(t)$. The transition peaks of the error
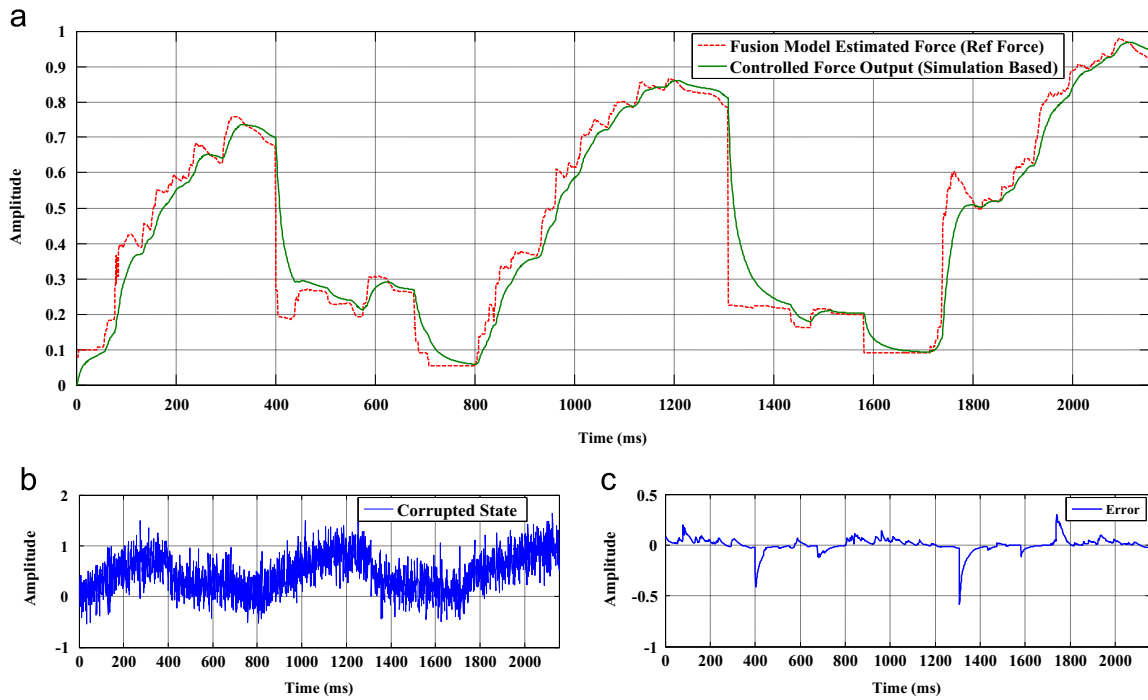
Fig. 10. The figure shows the non-real-time performance of LQG controller. (a) Validation plot for different model estimated forces with time index on x-axis and force in Newtons on y-axis. (b) Band limited white noise corrupted signal state, (c) error between the model reference and the simulation based forces during the grasping action. (a) Validation Plot, (b) Controller State and (c) Error.
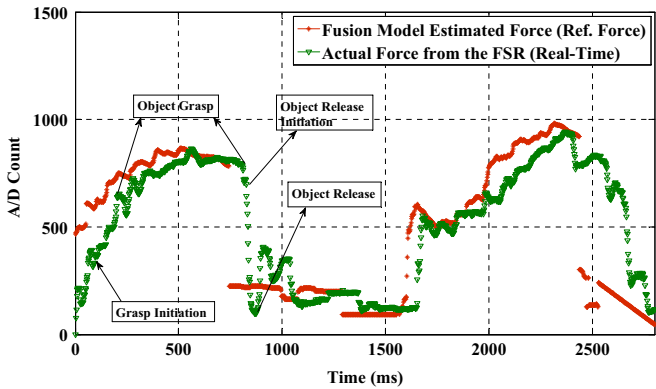

Fig. 11. OLMFA based force estimate and actual force from the force sensor mounted on the stress ball during the grasp.
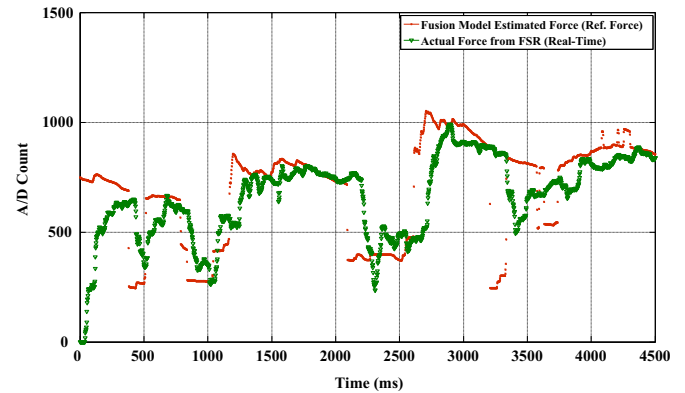

Fig. 12. OLMFA based force estimate and actual force from force sensor during the grasp for a different test subject.

as shown in Figs. 9c and 10c, relates to the relatively slow transient response of the proposed control system.

5.2. Real-time implementation

Fig. 11 shows the fusion model estimated force $\hat{Y}$ and actual force (Y) from the force sensor plotted together in the real-time grasping scenario. Fig. 11 also demonstrates detailed online grasping actions: GI, OG, ORI, OR. While conducting the experiment, the prosthetic hand prototype is utilized to maintain a minimum constant force throughout the grasping action, to ensure contact between the force sensor and the object. The same experiment is repeated to test the consistency and to make sure that the object is in contact with the force sensor throughout the grasping action.

Fig. 12 shows the repeated experimental results with a different reference force profile $\hat{Y}(t)$. The LQG controller is tracking the reference force profile $\hat{Y}(t)$ and matching the actual force (Y) with the model estimated force ($\hat{Y}$). The reference force profile is made as random as possible by feeding the sEMG signals acquired when

the test subject is made to do a random grasping action over a period of time. The acquired sEMG signals are fed into the MISO transfer function $H(z)$ to test the accuracy and the performance of the controller, while performing the random grasping action. Hence this robustness enables the prosthetic hand to effectively control the finger force while handling delicate objects.

During the experiments, the following observations were made: (i) Even though a lot of attention had been paid in choosing the DC motors with a fast time response, we observed slight delays in tracking the reference force profiles $\hat{Y}(t)$. In this work, the DC motors are solely responsible for the movement of the fingers and maintaining force. A relatively high transmission ratio is used and may contribute to the fact that the transient response is somewhat sluggish. In addition, the identified models that are responsible for modeling the output based on the measured sEMG signals, may have good steady-state performance, but are lacking in predicting the transient behavior. This indicates that there are instances in which the fingertip lost contact due to the high transmission ratio

and/or the sub-par transient response performance of the controller. However, the actual force from the force sensor (Y) tracks the changes in the reference force profile ($\hat{Y}$) very closely, except in the scenarios where the force changed drastically. Thus we can conclude that, apart from the fast changes in the transient response, the implemented control scheme produced promising results. (ii) It is also evident from Figs. 11 and 12 that the minimum constant force is needed to maintain contact with the object and also to accomplish accuracy in tracking the reference force profile. In order to test the precision of the proposed LQG controller, 18 different experiments are conducted with the k-fold cross validation data from the 18 test subjects. For the 18 experiments, the mean percentage Pearson's correlation coefficient of 91.6% and the mean percentage relative error of 9.2% with a standard deviation of ± 1.4 and ± 1.3 respectively, is achieved for the fusion model estimated force ($\hat{Y}$) and the actual force (Y). Because of the above mentioned transmission problems, measurement/model errors and the slow transient response of the controller, slight variability is observed in the correlation coefficients for the 18 experiments.

Fig. 13 depicts the validation plot with a different OLMFA based force estimate $\hat{Y}$(obtained by feeding a k-fold cross validation sEMG signals to the MISO transfer function ($H(z)$) and the actual force (Y). The same measurement/model errors and transient response problems are observed in this experiment. However, the controller tracks the reference force profile, the Pearson's correlation coefficients for the fusion model estimated force ($\hat{Y}$) and the actual force (Y) is 0.9, which is close to other experiments.

5.3. Comparison of OLMFA based LQG with and without rate partitioning

Table 1 provides the performance of the fusion algorithm based skeletal muscle force estimation and the LQG control scheme on the embedded framework with and without rate partitioning. Rate partitioning helps to achieve a better performance in both the skeletal muscle force estimation and control with more CPU utilization of the PIC 32MX360F512L. The embedded framework

with rate partitioning is able to achieve better performance without any task overruns.

Therefore the PIC 32 is able to handle computational load of rate partitioning and hence the authors choose to use rate partitioning on the embedded frame work and the OLMFA estimation and LQG control scheme results presented are from the rate partitioned embedded framework.

5.4. Comparison of OLMFA based LQG and MRAC schemes

The LQG control scheme is compared against a Model Reference Adaptive Control algorithm (MRAC) (⟨http://www.delsys.com/Products/Bagnoli_Desktop.html⟩) that was previously developed by the authors. The rate partitioning was not done for the MRAC, hence all the I/O's, skeletal muscle force estimation and the controller runs at the same time step on the embedded framework. This implementation caused increased grasping action delays in following the reference force profile which reflects as one reason for the reduced mean percentage correlation coefficients between the MRAC based actual and the estimated force in Table 2. The fusion algorithm based skeletal muscle force estimation and the LQG controller scheme with rate partitioning yields better correlation and less relative error between the fusion model estimated force profile ($\hat{Y}$) and the actual force (Y) than the MRAC. The correlation coefficient is increased by 10% and the relative error is decreased by 8% with a low Standard Deviation (SD) for the fusion algorithm based skeletal muscle force estimation and the LQG controller scheme with rate partitioning.

To test the variability of the results, cross validation is done. Table 2 provides the mean and standard deviation of the percentage correlation (ρ) and the relative error (η) for k-fold cross validation data from 18 subjects.M_2 is the model constructed from the k-fold cross validation sensor data $u_2(t)$ located on the motor unit whereas M_1 and M_3 are constructed from k-fold cross validation data sensor data $u_1(t)$ and $u_3(t)$ respectively adjacent to the motor unit. Using the k-fold cross validation, data from each sensor is divided into 18 different subsets. Each individual model M_1, M_2 and M_3, the OLMFA based estimates and the control schemes (LQG and MRAC) are
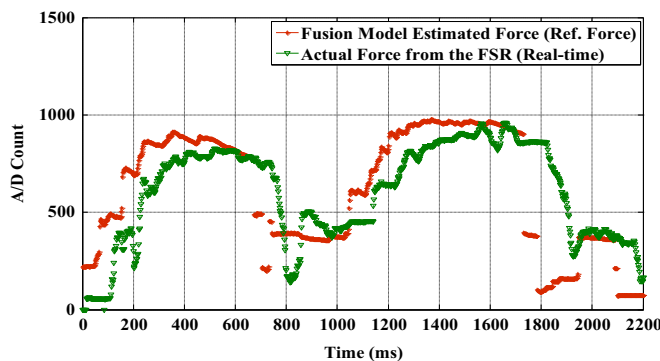

Fig. 13. Validation plot for OLMFA based force estimate and actual force from force sensor during the grasp (separate experiment).

Table 1
Fusion algorithm estimation, LQG scheme real-time performance and the PIC 32 CPU utilization on the embedded framework with and without rate partitioning, the values are based on the A/D count and the errors are based on the difference of the A/D count between the measured and predicted values.

Fusion algorithm						LQG control scheme					
With rate partition			Without rate partition			With rate partition			Without rate partition		
$\mu_\rho \pm \sigma_\rho$	$\mu_\eta \pm \sigma_\eta$	Load	$\mu_\rho \pm \sigma_\rho$	$\mu_\eta \pm \sigma_\eta$	Load	$\mu_\rho \pm \sigma_\rho$	$\mu_\eta \pm \sigma_\eta$	Load	$\mu_\rho \pm \sigma_\rho$	$\mu_\eta \pm \sigma_\eta$	Load
85.6 ± 1.6	20.4 ± 1.5	30.3 ± 0.03	80.3 ± 1.7	25.8 ± 1.6	42.3 ± 0.07	91.6 ± 1.4	9.2 ± 1.3	50.7 ± 0.01	86.1 ± 1.4	15.0 ± 1.5	40.4 ± 0.04

Table 2

Correlation coefficient percentages and percentage relative error between different predicted dynamic finger force levels and actual measured forces. The values are based on the A/D count and the errors are based on the difference of the A/D count between the measured and predicted values.

Subjects	Fusion algorithm results									MRAC $\rho_{X,Y}$	H	L_{MRAC}	LQG $\rho_{X,Y}$	H	L_{LQG}
	M_1		M_2		M_3		$\hat{Y}$								
	$\mu_\rho \pm \sigma_\rho$	$\mu_\eta \pm \sigma_\eta$	$\mu_\rho \pm \sigma_\rho$	$\mu_\eta \pm \sigma_\eta$	$\mu_\rho \pm \sigma_\rho$	$\mu_\eta \pm \sigma_\eta$	$\mu_\rho \pm \sigma_\rho$	$\mu_\eta \pm \sigma_\eta$	L_{FA}						
1	57.7 ± 1.9	50.3 ± 1.9	67.7 ± 1.8	45.2 ± 1.8	56.5 ± 1.9	48.9 ± 1.9	84.3 ± 1.6	28.8 ± 1.7	22.4 ± 0.04	84.0 ± 1.5	22.6 ± 1.4	19.8 ± 0.04	93.2 ± 1.2	15.8 ± 1.2	50.1 ± 0.01
2	52.6 ± 1.9	53.4 ± 1.9	59.3 ± 1.8	43.0 ± 1.8	50.0 ± 1.9	45.2 ± 1.8	82.2 ± 1.7	26.0 ± 1.6	23.6 ± 0.05	83.4 ± 1.5	24.7 ± 1.5	19.4 ± 0.03	90.2 ± 1.2	18.5 ± 1.2	51.4 ± 0.02
3	63.3 ± 1.8	53.1 ± 1.9	68.1 ± 1.9	41.7 ± 1.8	65.5 ± 1.9	48.8 ± 1.9	84.9 ± 1.7	26.2 ± 1.7	23.2 ± 0.03	84.5 ± 1.6	25.0 ± 1.4	19.9 ± 0.03	89.9 ± 1.1	17.9 ± 1.2	50.6 ± 0.02
4	66.1 ± 1.9	51.0 ± 1.9	67.6 ± 1.8	42.3 ± 1.8	64.0 ± 1.8	47.3 ± 1.9	83.8 ± 1.6	29.1 ± 1.7	23.3 ± 0.03	82.9 ± 1.4	25.2 ± 1.5	20.3 ± 0.03	90.5 ± 1.2	16.4 ± 1.3	50.3 ± 0.01
5	60.2 ± 1.9	50.4 ± 1.9	62.8 ± 1.8	44.9 ± 1.8	58.9 ± 1.9	49.2 ± 1.9	83.0 ± 1.6	30.0 ± 1.6	24.6 ± 0.04	85.2 ± 1.5	25.8 ± 1.5	18.6 ± 0.03	91.3 ± 1.2	17.4 ± 1.3	51.2 ± 0.01
6	59.5 ± 1.9	48.7 ± 1.9	66.9 ± 1.8	42.1 ± 1.8	61.8 ± 1.9	48.7 ± 1.9	84.0 ± 1.6	28.7 ± 1.6	23.1 ± 0.03	82.2 ± 1.5	23.1 ± 1.5	19.7 ± 0.03	92.2 ± 1.2	19.5 ± 1.3	50.8 ± 0.01
7	59.2 ± 1.9	46.3 ± 1.9	68.6 ± 1.8	40.9 ± 1.8	60.2 ± 1.9	45.8 ± 1.9	85.3 ± 1.6	26.2 ± 1.6	23.3 ± 0.03	85.9 ± 1.5	24.8 ± 1.5	19.9 ± 0.03	90.2 ± 1.2	18.2 ± 1.2	50.4 ± 0.01
8	57.4 ± 1.9	48.9 ± 1.8	64.7 ± 1.8	43.6 ± 1.8	55.2 ± 1.9	47.8 ± 1.9	83.7 ± 1.6	28.0 ± 1.6	23.8 ± 0.04	84.3 ± 1.4	23.7 ± 1.5	20.5 ± 0.03	90.6 ± 1.2	16.5 ± 1.2	51.3 ± 0.01
9	58.3 ± 1.8	47.2 ± 1.9	66.2 ± 1.8	42.3 ± 1.8	54.4 ± 1.9	50.0 ± 1.9	84.3 ± 1.5	29.3 ± 1.6	24.9 ± 0.04	83.1 ± 1.5	24.8 ± 1.5	19.7 ± 0.04	90.5 ± 1.2	18.7 ± 1.2	50.6 ± 0.01
10	60.5 ± 1.9	49.7 ± 1.9	65.7 ± 1.8	43.3 ± 1.8	62.9 ± 1.9	47.1 ± 1.9	85.0 ± 1.6	27.1 ± 1.6	23.1 ± 0.04	85.7 ± 1.5	23.5 ± 1.5	19.3 ± 0.03	91.4 ± 1.2	17.6 ± 1.2	50.0 ± 0.01
11	54.8 ± 1.9	48.7 ± 1.9	57.2 ± 1.9	44.1 ± 1.9	52.9 ± 1.9	51.9 ± 1.8	83.0 ± 1.7	26.0 ± 1.7	23.5 ± 0.03	83.5 ± 1.5	24.2 ± 1.5	19.6 ± 0.03	90.2 ± 1.2	16.2 ± 1.2	50.2 ± 0.01
12	63.7 ± 1.9	47.3 ± 1.9	69.3 ± 1.8	41.2 ± 1.8	59.8 ± 1.9	50.0 ± 1.8	84.9 ± 1.6	25.4 ± 1.7	23.4 ± 0.03	84.4 ± 1.5	24.9 ± 1.5	19.2 ± 0.03	90.9 ± 1.2	18.4 ± 1.2	50.5 ± 0.01
13	58.3 ± 1.8	50.2 ± 1.9	65.0 ± 1.8	45.2 ± 1.8	54.3 ± 1.9	49.6 ± 1.9	84.5 ± 1.6	27.1 ± 1.6	23.0 ± 0.03	84.2 ± 1.5	23.0 ± 1.5	19.0 ± 0.03	90.3 ± 1.2	17.6 ± 1.3	50.7 ± 0.01
14	59.8 ± 1.9	48.1 ± 1.8	61.2 ± 1.8	43.2 ± 1.8	56.3 ± 1.9	48.6 ± 1.9	84.7 ± 1.6	29.0 ± 1.6	22.4 ± 0.03	84.9 ± 1.5	22.1 ± 1.4	19.8 ± 0.04	90.8 ± 1.2	17.8 ± 1.3	50.6 ± 0.01
15	59.4 ± 1.9	50.4 ± 1.8	66.0 ± 1.8	45.6 ± 1.8	51.3 ± 1.9	49.8 ± 1.9	83.9 ± 1.6	27.6 ± 1.6	23.7 ± 0.03	83.1 ± 1.5	24.9 ± 1.4	19.5 ± 0.03	91.9 ± 1.1	16.5 ± 1.2	50.3 ± 0.02
16	58.7 ± 1.9	47.1 ± 1.9	64.4 ± 1.8	41.2 ± 1.8	53.9 ± 1.9	47.0 ± 1.8	84.4 ± 1.6	28.7 ± 1.7	23.5 ± 0.03	84.7 ± 1.5	23.6 ± 1.5	19.4 ± 0.03	90.5 ± 1.2	18.6 ± 1.2	50.9 ± 0.01
17	55.2 ± 1.9	49.0 ± 1.9	68.1 ± 1.8	43.2 ± 1.8	54.3 ± 1.9	45.8 ± 1.9	84.0 ± 1.5	26.4 ± 1.6	23.6 ± 0.04	84.9 ± 1.5	22.7 ± 1.5	19.1 ± 0.03	90.6 ± 1.2	16.5 ± 1.3	50.4 ± 0.01
18	58.9 ± 1.9	48.9 ± 1.9	65.2 ± 1.9	44.2 ± 1.8	60.7 ± 1.9	49.0 ± 1.9	85.2 ± 1.6	29.4 ± 1.6	23.1 ± 0.04	85.8 ± 1.5	24.5 ± 1.5	19.8 ± 0.03	91.4 ± 1.2	17.3 ± 1.2	50.6 ± 0.01

validated with the k-fold cross validation subset data from the 18 subjects. Therefore the mean and standard deviation of the percentage correlation and the relative error for each individual model, the fusion estimates and the controller's performance for 18 k-fold validation subset data are presented in Table 2.

From Table 2 it can be inferred that the sensor data fusion improves the percentage correlation (ρ) and reduces the percentage relative error (η) between the actual force ($Y(t)$) and the fusion algorithm estimated force ($\hat{Y}_f$) when compared to individual model force estimates. It can also be inferred from Table 2 that M_2 (bold & italic) is performing better than M_1 and M_3 for the cross validation data. It is also observed that the standard deviation for the percentage relative error and the percentage correlation is low for M_2 when compared with other models M_1 and M_3. Therefore, it can be inferred that the sensor located directly on the motor point is giving data that is more suitable to extract useful information from when compared with the other sensory data. M_1 (underlined & italic) is yielding the next best performance when compared with M_3 except for subjects 3, 6, 10 and 18 (underlined & italic). This could be due to motor point location in reference to sensor alignment and crosstalk and noise interference. It is observed from Table 2 that the LQG controller is performing better than the MRAC for all 18 subjects' k-fold validation data in terms of high mean percentage correlation, low percentage relative error and standard deviation (bold). Table 2 also indicates the percentage mean CPU utilization (L) of the PIC 32MX360F512L for 18 subject's k-fold cross validation for both the MRAC and LQG control schemes respectively. Although, the LQG control scheme is computationally expensive to implement on a real-time embedded test platform, it yields precise and accurate finger force control of the prosthetic hand. Thus, in order to preserve accuracy, the LQG controller demands a higher performance embedded platform in terms of computing power.

5.5. Comparison with the existing literature

In Lopez et al. (2009), Variance Weighted Average (VWA) and decentralized Kalman filter (DKF) based data fusion algorithms were implemented and tested on five volunteers. The results were compared based on the absolute error. Because of the dynamic nature of the EMG signal and the variability between test subjects, the reporting of the absolute error can lead to false conclusions. Therefore, in this work, the relative error is primarily used for quantitative analysis of the proposed fusion algorithm. The proposed fusion algorithm is tested with the k-fold cross validation data obtained from 18 test subjects, demonstrating a consistent improvement in estimating the skeletal muscle force when compared to the individual model estimated force. Since the literature doesn't seem to be abundant in the data fusion for sEMG signals, it is difficult to make an extensive quantitative comparison of the previous research with the current work.

A real-time control of upper extremity prostheses was studied using a sonomyography (SMG) signal from the amplitude of the muscle deformation to control the prosthetic hand (Jun et al., 2010). The utilized two-dimensional logarithmic search (TDL) prosthesis control algorithm yielded an overall mean correlation coefficient of 0.99 and a mean root-mean-square < 0.75 for a 1-degree of freedom (DOF) prosthetic hand. The real-time performance of the algorithm is not evaluated. A real-time control of a virtual hand study was done by using a local approximation with lazy learning (Sebelius et al., 2005). The experiments were carried out on six healthy male subjects. In Kazuo and Yoshiaki (2012) an EMG based impedance control method was proposed to control the robotic hand using a neuro-fuzzy matrix modifier to make the controller adaptable for the intended motion. The user's hand force vector is calculated based on the estimated joint torque and user's hand acceleration is obtained based on the calculated hand force vector to estimate the user's hand trajectory using neuro-fuzzy classifier.

However, the neuro-fuzzy just like the HILL model (Mitsuhiro and David, 2013), is intolerant to the subject's variability. The proposed SI approach in this manuscript has subject variability tolerance which is proved by the k-fold cross validation. The other approaches in achieving real-time sEMG based control of upper extremity prostheses is by utilizing real-time intelligent classifiers (Nishikawa et al., 2001; Englehart et al., 2001; Christian et al., 2011). However, the classification does not provide dynamic sEMG/skeletal muscle force estimation such as the SI approach and limits the functionality of the prostheses to certain pre-programmed grasping actions.

6. Conclusion and future work

In this work, a two-stage real-time rate partitioned embedded framework was designed for estimation and control of the finger force of the prosthetic hand prototype. Half-Gaussian and Chebyshev type-II filters were utilized for the sEMG and skeletal muscle force filtration. System identification (SI) technique is utilized to model the dynamic relationship between sEMG–force by employing linear Output-Error (OE) models. Although better individual models can be inferred using SI under perfect conditions, the OLMFA improves the predicted force estimate consistently. The fusion algorithm's results were consistent for all the test subjects. The results indicate that the OLMFA yields a mean percentage correlation of 85.6% and a mean percentage relative error of 20.4% with a mean standard deviation of ± 1.6 and ± 1.5, respectively. A real-time LQG controller is designed to achieve the finger force control of the upper extremity prosthesis. The LQG controller based force output and actual force output for the k-fold cross validation data of 18 test subjects tested on the rate partitioned embedded framework yields a mean percentage correlation of 91.6% and a mean percentage relative error of 9.2% with a mean standard deviation of ± 1.4 and ± 1.3 respectively. The proposed LQG control scheme yielded desirable correlations with a low relative error when compared with a MRAC scheme. From the results it is also evident that the proposed design takes care of the force overshoot problems such as those of the Motion Hand (Toledo et al., 2009). The OLMFA skeletal muscle force estimation and the control scheme is tested with the index finger data from the 18 test subjects and can be easily extended to the rest of the fingers with a suitable EMG sensor array. The proposed OLMFA estimation and the controller scheme achieved the real-time performance on the rate partitioned embedded framework with a mean CPU utilization of 81% with a standard deviation of ± 0.02 for 18 different experiments. The embedded framework is capable of transmitting the data from the PIC 32 CPU to the computer. This enables us to validate the performance of the controller design and also allows fast trouble shooting with real hardware. This kind of semi-autonomous real-time control system for the prosthetic hand can substitute for vibrotactile feedback. Although this design doesn't provide any feedback directly to the amputee, the intelligent sEMG fusion algorithm along with the semi-autonomous control system can take care of the grasping actions by having a fine control of finger force along with visual feedback by the amputee.

The sEMG based finger force OE models are constructed based on the normal limb sEMG and the corresponding force measurements with the idea of extracting the dynamic relationship between sEMG and skeletal muscle force. These dynamic models can be mapped to an amputee who has a variable amount of residual musculature, varying levels of atrophy, and an unknown force output by recalibrating the models with the sEMG data using an existing limb or standard force models (in case of multiple limb amputation). This design can also be extended to above elbow amputations by approximating the sEMG data from the biceps and triceps motor points. This aspect of research is one of our future goals. Also, the proposed fusion algorithm and the semi-autonomous control strategy can be generalized and have versatile applications in the humanoid robotics, computational intelligence and brain computer interface (BCI).

There is a clear advantage of superior sEMG–skeletal muscle force estimation with three sEMG sensors as shown in Table 2. Although the superior skeletal muscle force estimation scheme poses some complexity in having three channels for each individual finger, it can be easily addressed by adding multiple lower level microcontroller/microprocessors for sEMG signal acquisition and analog to digital conversion, when we extend it to the five fingers. Further, the better estimation compensates for the complexity due to multiple channels. This presented research is not only confined to bio-medical applications but also has extensive applications in computational intelligence, machine learning, uncertainty analysis etc. The idea of acquiring more sEMG signals by utilizing multiple sensors for the purpose of inferring more information about finger forces is shown as a valid approach in this work. Hence, utilizing three or more EMG channels is feasible and from the results presented provides an improved estimate.

Acknowledgment

Appendix A

The resulting MISO transfer function $H(z)$ is constructed as follows:
From u_1 to output,

$$\frac{z^8 - 3.843z^7 + 7.729z^6 - 10.78z^5 + 10.6z^4 - 7.417z^3 + 3.603z^2 - 0.9795z + 0.1192}{z^8 - 4.028z^7 + 6.325z^6 - 4.121z^5 - 1.545z^4 + 5.87z^3 + 2.28z - 0.3496} \quad (A.1)$$

From u_2 to output,

$$\frac{z^8 - 4.339z^7 + 9.005z^6 - 12.42z^5 + 12.22z^4 - 8.117z^3 + 3.427z^2 - 0.557z + 0.0958}{z^8 - 4.028z^7 + 6.325z^6 - 4.121z^5 - 1.545z^4 + 5.87z^3 - 5.433z^2 + 2.28z - 0.349} \quad (A.2)$$

From u_3 to output,

$$\frac{z^8 - 3.522z^7 + 6.655z^6 - 8.864z^5 + 8.183z^4 - 5.365z^3 + 2.423z^2 - 0.557z + 0.0958}{z^8 - 4.028z^7 + 6.325z^6 - 4.121z^5 - 1.545z^4 + 5.87z^3 - 5.433z^2 + 2.28z - 0.349} \quad (A.3)$$

Pearson correlation coefficient is given by

$$\rho_{X,Y} = \mathrm{corr}(X,Y) = \frac{\mathrm{cov}(X,Y)}{\sigma_X \sigma_Y} = \frac{E\left[(X - \mu_X)(Y - \mu_Y)\right]}{\sigma_X \sigma_Y} \quad (A.4)$$

where X, Y are random variables, μ_x and μ_y are expected values, and σ_x, σ_y are standard deviations respectively. E is the expected value operator.

Relative Error is given by

$$\eta = \frac{\Delta x}{x} \quad (A.5)$$

where x is the measured value and Δx is the absolute error

LQG Algorithm with computational cost:
The following color coding is utilized to represent the computational expense of the LQG algorithm.

■ - Addition (Add)

■ - Subtraction (Sub)

■ -Multiplication (Mul)

■ - Division (Div)

■ - Matrix Manipulation (MM)

Step 1: Enter the prior estimate $\hat{x}_k^-$ and its error covariance P_k^-.
Step 2: Compute the Kalman estimator (filter) gain

$$K_{ek} = P_{ek}^- H_k' [H_k P_{ek}^- H_k' + R_k]^{-1} = P_{ek} H_k' (R_k')^{-1} \qquad (A.6)$$

| 1 | 9 | 2 | 4 |
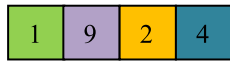
where $P_{ek} = [1 - K_{ek}H_k]P_{ek}'$
P_{ek} is the $n \times n$ state estimation covariance error matrix
Step 3: Update estimates with measurement y_k,

$$\hat{x}_k = \hat{x}_k' + K_{ek}[y_k - H_k\hat{x}_k^-]. \qquad (A.7)$$

| 1 | 1 | 3 | 1 |

Step 4: Project ahead the state as

$$\hat{x}_{k+1}^- = F_k\hat{x}_k + G_k u_k \qquad (A.8)$$

| 1 | 2 |

Step 5: Project ahead the error covariance as

$$P_{e(k+1)}^- = F_k\hat{x}_k + G_k u_k, \qquad (A.9)$$

| 1 | 2 |

$$P_{ek}' - K_{ek}[H_k P_{ek}^- H_k' + R_k]K_{ek}' \qquad (A.10)$$

| 1 | 1 | 5 | 2 |

Step 6: Go to Step 2 and repeat.
To find the best optimal control,
Step 7: Solve the matrix difference Riccati equation

$$P_k = F_k' \left[\begin{array}{c} P_{k+1} - \\ P_{k+1}G_k[G_k'P_{k+1}G_k+R_k]^{-1}G_k'P_{k+1} \end{array} \right] F_k + Q_k, \qquad (A.11)$$

| 2 | 1 | 9 | 1 | 2 |

with the final condition $P(k = k_f) = F_{kf}$. The Ricatti equation is solved offline using the QZ algorithm and the coefficients are used in the real-time implementation.
Step 8: With the solution of P_k from Step 7, obtain the optimal Kalman controller gain as

$$K_k = [G_k'P_{k+1}G_k + R_k]^{-1}G_k'P_{k+1}F_k \qquad (A.12)$$

| 1 | 5 | 1 | 2 |

Step 9: The optimal control u_k is given by

$$u_k = -K_k\hat{x}_k. \qquad (A.13)$$

| 1 |

References

Aca News: National Limb Loss Awareness Month,2011. Available: ⟨http://www.bocusa.org/aca-news-national-limb-loss-awareness-month⟩.
Anthony L.C., Molitor J., Perez G.A., Chiu S.C., 2010. Design of a robotic hand and simple EMG input controller with a biologically-inspired parallel actuation system for prosthetic applications. In: ASME 2010 International Design Engineering Technical Conference & Computers and Information in Engineering Conference.
Anugolu M., Sebastian A., Kumar P., Schoen M.P., Urfer A., Naidu D.S., 2009. Surface EMG array sensor based model fusion using Bayesian approaches for prosthetic hands. In: ASME 2009 Dynamic Systems and Control Conference, Hollywood: CA, USA. http://dx.doi.org/10.1115/DSCC2009-2690.
Biddiss, E.A., Chau, T.T., 2007. Upper limb Prosthesis use and abandonment: a survey of the last 25 years. Prosthet. Orthot. Int. 3 (3), 236–257.
Bien, z.z., stefanoy, D., 2004. Advances in rehabilitation robotics: human-friendly technologies on movement assistance and restoration for people with disabilities. Adv. Rehabil. Rob. 306, 3–23.
Causalities in Afghanistan & Iraq. ⟨www.unknownnews.net⟩, June 5, 2006.
Christian, C., Christian, A., Marco, C., Goran, L, Brigitta, R., Maria, C.C., Fredrik, S., 2011. Online myoelectric control of dexterous hand prosthesis by transradial amputees. IEEE Trans. Neural Syst. Rehabil. Eng. 19 (3), 260–270. http://dx.doi.org/10.1109/TNSRE.2011.2108667.
Clynes, M, Milsum, J.H., 1970. Biomedical Engineering Systems. McGraw-Hill, New York, NY, pp. 489–549.
Cram, J.R., Kasman, G.S., Holtz, J., 1998. Introduction to Surface Electromyography. Aspen Publisher Inc, Gaithersburg, MD.
Englehart, K., Hudgins, B., Parker, P.A., 2001. A wavelet-based continuous classification scheme for multifunction myoelectric control. IEEE Trans. Biomed. Eng. 48 (3), 302–311. http://dx.doi.org/10.1109/10.914793.
Esquenazi, A., Meire, R.H., 1996. Rehabilitation in limb deficiency for limb amputation. Arch. Phys. Med. Rehabil. 77 (3), 18–28.
Fougner, A., Staydahl, O., Kyberd, P.J., Losier, Y.G., Parker, P.A., 2012. Control of upper limb prostheses: terminology and proportional myoelectric control—a review. IEEE Trans. Neural Syst. Rehabil. Eng. 20 (5), 663–677. http://dx.doi.org/10.1109/TNSRE.2012.2196711.
Heinzmann, J., Zelinsky, J., 1999. A safe-control paradigm for human–robotic interaction. J. Intell. Rob. Syst. 25 (4), 295–310. ⟨http://www.delsys.com/Products/Bagnoli_Desktop.html⟩.
Interlink Electronics. FSR 402 Data sheet. Available: ⟨www.interlinkelectronics.com⟩.
Istenic R, Holobar A, Merletti R, Zazula D, 2007. EMG Based muscle force estimation using motor unit twitch model and convolution Kernel Compensation. In: 11th Mediterranean Conference on Medical and Biomedical Engineering and Computers, IFMBE Proceedings, vol. 16, pp. 114–117. http://dx.doi.org/10.1007/978-3-540-73044-6-29.
Jun, S., Qian, C., Yong-Ping, Z., 2010. Feasibility of controlling prosthetic hand using sonomyography signal in real-time: preliminary study. J. Rehabil. Res. Dev. 47 (2), 87–98.
Karl, J.A., Bjorn, W., 2008. Adaptive Control, second ed. Dover Publications.
Kaveh, M., Sridhar, K., Tom, C., 2007. Real-time classification of forearm electromyographic signals corresponding to user-selected intentional movements for multifunction prosthesis control. IEEE Trans. Neural Syst. Rehabil. Eng. 15 (4), 535–542. http://dx.doi.org/10.1109/TNSRE.2007.908376.
Kazuo, K., Yoshiaki, H., 2012. An EMG-based control for an upper-limb power-assist exoskeleton robot. IEEE Trans. Syst. Man Cybern. 42 (4), 1064–1068. http://dx.doi.org/10.1109/TSMCB.2012.2185843.
Kwang-Hoon, K., Gyu-In, J., Jong-Hwa, S., 2008. The stability of the adaptive two-stage extended Kalman filter. Int. Conf. Control Autom. Syst., 1378–1383. http://dx.doi.org/10.1109/ICCAS.2008.4694358.
Kyberd, P.J., Hill, W., 2011. Survey of upper limb prosthesis users in Sweden, the United Kingdom and Canada. Prosthet. Orthot. Int. 35 (2), 234–241.
Liberating Technologies Holliston MA, 2011. Available: ⟨http://www.liberatingtech.com/⟩.
Lopez, N.M., Di Sciasci, F., Soria, C.M., Valentinuzzi, M.E., 2009. Robust EMG sensing system based on data fusion for myoelectric control of a robotic arm. Biomed. Eng. Online 8, 5. http://dx.doi.org/10.1186/1475-925X-8-5.
Merletti R. Standards for Reporting EMG Data, International Society of Electrophysiology and Kinesiology. Available: ⟨http://www.isek-online.org/standards_emg.html⟩. February 1999; 9(1):III-IV.

Merrill, D.R., Lockhart, J., Troyk, P.R., Weir, R.F, Hankin, D.L., 2011. Development of an implantable myoelectric sensor for advanced prosthetics control. Artif. Organs 3.5 (3), 249–252.

Mitsuhiro, H, David, G, 2013. Voluntary EMG-to-force estimation with a multi-cscale physiological model. Biomed. Eng. Online 12, 86. http://dx.doi.org/10.1186/1475-925X-12-86.

Motion Control, Salt Lake City, UT, 2011. Available: ⟨http://www.utaharm.com/⟩.

Naidu, D.S., 2002. Optimal Control Systems. CRC Press, Boca Raton, FL.

Naidu, D.S., Chen, C.H., 2011. Control Strategies for Smart Prosthetic Hand Technology: An Overview, Book Chapter 14, Distributed Diagnosis and Home Healthcare (D2H2). American Scientific Publishers, CA.

Nishikawa, D., Yu, W., Yokoi, H., Kakazu, Y., 2001. Online learning method for EMG prosthetic hand control. Electron. Commun. Jpn. 84 (10), 1510–1519. http://dx.doi.org/10.1002/ecjc.1040.

Otto Bock Duderstadt, Germany, 2011. Available: ⟨http://www.ottobock.com/⟩.

Potluri C., Kumar P., Anugolu M., Urfer, A., Chiu S., Naidu D.S., Schoen M.P., 2010. Frequency Domain Surface EMG Sensor Fusion for Estimating Finger Forces. In: 32nd Annual International Conference of the IEEE Engineering in Medicine and Biology Society, pp. 5975–5978. http://dx.doi.org/10.1109/IEMBS.2010.5627575.

Potluri C., Anugolu M., Yihun Y., Jensen A., Chiu S., Schoen M.P., Naidu D.S., 2011. Optimal tracking of a sEMG based force model for a prosthetic hand. In: 33rd Annual International Conference of the IEEE Engineering in Medicine and Biology Society, Boston: MA, USA. pp. 1604–1607. http://dx.doi.org/10.1109/IEMBS.2011.6090464.

Puchhammer G., 2000. The Tactile Slip Sensor: Integration of a Miniaturized Sensory Device on Myoelectric Hand, Orthopadie-Technik Quarterly, English, edition I/2000. pp. 7–12.

RSL Steeper Leeds, U.K., 2011. Available: ⟨http://www.rslsteeper.com/⟩.

Raez, M.B.I., Hussain, M.S., Mohd-Yasin, F., 2006. Techniques of EMG signal analysis: detection, processing, classification and application. Biomed. Proced. Online 8, 11–35. http://dx.doi.org/10.1251/bpo115.

Railbert, M.H., Craig, J.J., 1981. Hybrid position and force control of manipulators. ASME J. Dyn. Syst. Meas. Control 102, 126–133.

Ruoyin Z., Jiting L., 2010. Kinematics and workspace analysis of an exoskeleton for thumb and index finger rehabilitation. In: IEEE International Conference on Robotics and Biomimetics, Tianjin, China. DOI: 10.1109/ROBIO.2010.5723307.

Sameni, R., Shamsollahi, M.B., Jutten, C., Babaie-Zadeh, M., 2005. Filtering noisy ECG signals using the extended Kalman filter based on a modified dynamic ECG model. IEEE Comput. Cardiol., 1017–1020. http://dx.doi.org/10.1109/CIC.2005.1588283.

Schoen, M.P., 2008. Application of genetic algorithms to Observe Kalman Filter Identification. J. Vib. Control 14 (7), 971–997.

Schwartz, M., 2012. EMG Methods for Evaluating Muscle and Nerve Function. InTech Publishers, ISBN: 978-953-307-793-2.

Sebelius, F., Axelsson, M., Danielsen, N., Schouenborg, J., Laurell, T., 2005. Real-Time Control of a Virtual Hand. 17. IOS Press, pp. 131–141.

Shanghai Kesheng Prostheses. 2011. Shanghai, China, 2011. Available: ⟨http://www.keshen.com/index-en.asp⟩.

Texas Instruments 1995. SN754410 Quadruple Half H-driver Data Sheet, Dallas, TX, November 1986 and 1995.

Toledo C., Leija L., Munoz R., Vera A., Ramirez A., 2009. Upper Limb Prostheses for Amputations Above Elbow: A Review, Health Care Exchanges, 2009 PAHCE. pp. 104–108. http://dx.doi.org/10.1109/PAHCE.2009.5158375.

Touch Bionics. Livingston, U.K., 2011. Available: ⟨http://www.touchbionics.com/⟩.

Widjaja, F., Shee, C.Y., Latt, W.T., Au, W.L., Poignet, P., Ang, W.T., 2008. Kalman filtering of accelerometer and electromyography (EMG) data in pathological tremor sensing system. IEEE Int. Conf. Rob. Autom., 3250–3255. http://dx.doi.org/10.1109/ROBOT.2008.4543706.

Wiener, N., 1948. CYBERNETICS or Control and Communication in the Animal and the Machine. MIT Press, Cambridge, MA.

Xiaoping, Y., Eric, R.B., 2006. Design, implementation, and experimental results of a quaternion-based Kalman filter for human body motion tracking. IEEE Trans. Rob. 22 (6), 1216–1227. http://dx.doi.org/10.1109/TRO.2006.886270.

Ziegler-Graham, K, MacKenzie, E.J., Ephraim, P.L., Travison, T.G., Brookmeyer, R., 2008. Estimating the prevalence of limb loss in the United States: 2005 to 2050. Arch. Phys. Med. Rehabil. 89 (3), 422–429.

Zinn, M., Roth, B., Khatib, O., Salisbury, J.K., 2004. A new actuation approach for human friendly robot design. Int. J. Rob. Res. 23 (4-5), 379–398.